Modelling and Operation Strategies of DLR's Large Scale Thermocline Test Facility (TESIS)

Christian Odenthal[1, a)], Nils Breidenbach[1, b)] and Thomas Bauer[2, c)]

[1] German Aerospace Center (DLR), Pfaffenwaldring 38-40, 70569 Stuttgart
[2] German Aerospace Center (DLR), Linder Höhe, 51147 Cologne

[a)] Corresponding author: christian.odenthal@dlr.de
[b)] nils.breidenbach@dlr.de
[c)] thomas.bauer@dlr.de

Abstract. In this work an overview of the TESIS:store thermocline test facility and its current construction status will be given. Based on this, the TESIS:store facility using sensible solid filler material is modelled with a fully transient model, implemented in MATLAB®. Results in terms of the impact of filler site and operation strategies will be presented. While low porosity and small particle diameters for the filler material are beneficial, operation strategy is one key element with potential for optimization. It is shown that plant operators have to ponder between utilization and exergetic efficiency. Different durations of the charging and discharging period enable further potential for optimizations.

INTRODUCTION

Thermocline thermal energy storages allow significant cost reductions by storing a liquid storage material inside a single tank, when compared to a two tank storage system. By embedding a low cost solid filler material, further cost reductions of up to 33 % can be achieved (*1*).

First experimental results in a large scale of 170 MWh_{th} of such a storage system have been tested at the SolarOne power plant (*2*). This system used thermal oil as HTF and rocks as filler material. Experimental results with molten salt, but in a smaller scale of 2.3 MWh_{th} have been presented by Sandia (*3*). Recently, Hoffmann et al. compared those results with their own experiments and investigated the impact of several modelling simplifications on the accuracy of their model. Mawire & McPherson (*4*) developed models in SIMULINK and compared them with their own lab scale experiments with thermal oil as HTF. A mid-sized experiment with 3 m height, 1 m diameter and thermal oil operating at up to 350 °C has been investigated at CEA (*5*).

At CIEMAT simplified models for system simulations (*6*) and possible operation strategies (*7*) have been theoretically investigated. A molten salt storage system with embedded heat exchanger for direct steam generation has been set up at ENEA (*8*) and was compared with a CFD model developed at CIEMAT (*9*). A single tank thermocline concept without filler material has been presented by SENER, where a floating barrier is used to prevent mixing of hot and cold salt (*10*). CEA has successfully demonstrated a complete plant, consisting of a fresnel collector, an organic rankine cycle (ORC) and a thermocline thermal storage (*11*).

At DLR in cologne, a large scale thermocline test facility with up to 22 m^3 storage volume is currently set up and expected to be operational by 2017 (*12*). Currently, the concrete foundation and the storage and reservoir tanks have been set up. An illustration of the planned storage volume (TESIS:store) is shown in Fig. 1 (a). A P&I diagram of the interconnection is shown in Fig. 1 (b). Every component has an electric trace heating to minimize heat losses to the environment. The storage volume can be equipped with up to 150 thermocouples, to allow measuring the three-dimensional temperature field on the inside.

On the inside of the tank, the filler material is held by a stack of three removable baskets. By this design, various test arrangements including instrumentation (i.e. thermocouples, strain gauges) can be prearranged on the outside

and later inserted into the storage tank. Hot and cold molten salt is provided by two reservoir tanks, whose temperatures can be individually adjusted. These reservoirs imitate the behavior of attached energy sources or sinks (i.e. heater, solar collector or power plant) and the pumps inserted in these two tanks can provide a molten salt mass flow of more than 14 tons/h at 560°C.

The operation of the plant can be described by the following example: During discharging, cold salt influxes at the bottom of the storage volume and flows through the filler material up to the top, where it is extracted. Heat is transferred from the hot filler material to the initially colder molten salt. The heat transfer is usually limited to a region between already cooled and yet hot filler material, which is called the thermocline zone. The thermocline zone slowly moves through the storage volume until it reaches the top. When this happens, the exit temperature of the hot salt will decline, having negative effects on the process attached to the storage system. Hence, a short thermocline is favorable, keeping the exit temperature at a constant level for as long as possible. Previous publications, dealing with the optimization of thermocline systems, confirm that operation strategy significantly affects the shape of the thermocline and eventually influences the thermal behavior of such thermocline system (*13*).

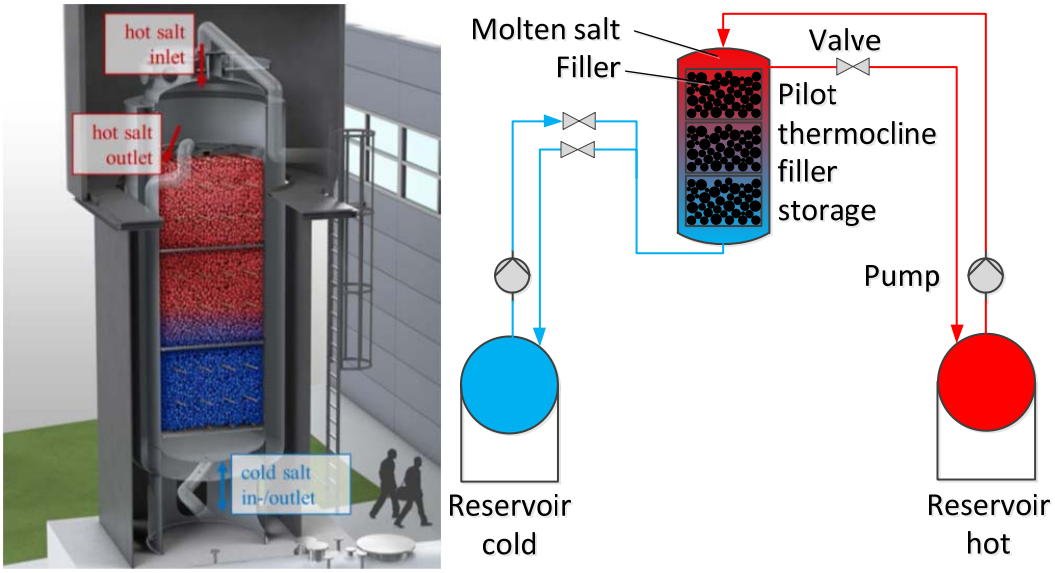

FIGURE 1. (a) Illustration of the planned TESIS:store test facility; (b) Simplified P&I diagram of the facility

For the TESIS:store test facility, the outer dimensions of the storage volume are fixed, but the geometry of possible filler materials and its operation strategy are subject to optimizations.

METHODOLOGY

In the following chapter, a computer model is described and used to identify possible filler materials and operation strategies.

Simplified Computer Model

For the investigations, a simplified model with fast execution speed is necessary. The model is based on the partial differential equations (PDE) of the temperature fields of the fluid and solid. For the fluid the transient term for the change in inner energy, the transport of thermal energy and the coupling with the solid are taken into account. Heat losses and conduction are neglected, since their influence is comparatively small, when considering large storage volumes being not on standby.

The fluid PDE then reads

$$\varepsilon \rho_{\mathrm{f}} c_{\mathrm{f}} \frac{\partial T_{\mathrm{f}}}{\partial t} = -\rho_{\mathrm{f}} c_{\mathrm{f}} v_{0,\mathrm{x,f}} \frac{\partial T_{\mathrm{f}}}{\partial x} + \dot{Q}_f{}''' \tag{1}$$

Here, ε denotes the porosity, $\rho_{\mathrm{f}} c_{\mathrm{f}}$ the volumetric heat capacity of the fluid, $v_{0,\mathrm{x,f}}$ the superficial flow velocity of the fluid and $\dot{Q}_f{}'''$ the energy from or to the solid. In terms of the solid there is only the transient change in inner energy and a coupling term with the fluid, hence the solid PDE reads

$$(1-\varepsilon) \rho_{\mathrm{s}} c_{\mathrm{s}} \frac{\partial T_{\mathrm{s}}}{\partial t} = \dot{Q}_{\mathrm{s}}{}'''. \tag{2}$$

The product $\rho_{\mathrm{s}} c_{\mathrm{s}}$ is the volumetric heat capacity of the solid and $\dot{Q}_{\mathrm{s}}{}'''$ the coupling term, which is calculated from

$$\dot{Q}_f{}''' = -\dot{Q}_s{}''' = k_{\mathrm{vol}} \cdot (T_{\mathrm{s}} - T_{\mathrm{f}}),$$
$$\text{where } k_{\mathrm{vol}} = \frac{1}{\alpha_{\mathrm{vol}}} + \frac{2\lambda}{5 \cdot d_{\mathrm{part}}} \tag{3}$$

is the effective heat transfer coefficient. The second term in k_{vol} takes the resistance arising from the conductivity of the solid λ into account and has been developed by Schmidt & Willmott (*14*).

The film heat transfer α_{vol} coefficient is calculated from a Nusselt-correlation derived by Wakao et al. (*15*):

$$Nu = 2 + 1.1 \cdot Pr^{\frac{1}{3}} \cdot Re_{\mathrm{part,PB}}^{0,6} = \frac{a_{\mathrm{v}} \cdot \alpha_{\mathrm{vol}} \cdot d_{\mathrm{part}}}{\lambda_{\mathrm{f}}} = \frac{6(1-\varepsilon) \cdot \alpha_{\mathrm{vol}}}{\lambda_{\mathrm{f}}}. \tag{4}$$

The specific surface per volume a_{v} is calculated from the porosity ε and the average particle diameter d_{part}

$$a_{\mathrm{v}} = \frac{6(1-\varepsilon)}{d_{\mathrm{part}}} \tag{5}$$

The pressure loss is calculated from Ergun's (*16*) equation:

$$\Delta p = \frac{L}{d_{\mathrm{part}}} \frac{(1-\varepsilon)}{\varepsilon^3} \left(\frac{150 \cdot (1-\varepsilon) \cdot \mu_{\mathrm{f}}}{\rho_{\mathrm{f}} v_{0,\mathrm{f}} \cdot d_{\mathrm{part}}} + 1{,}75 \right) \rho_{\mathrm{f}} v_{0,\mathrm{f}}^2 \tag{6}$$

To solve the PDEs, a spatial discretization is applied, leading to a set of ordinary differential equations (ODEs), which are discretized by an implicit scheme with respect to time. This leads to a system of linear dependent equations which can be described by

$$\bar{\bar{\boldsymbol{M}}} \cdot \boldsymbol{T}^{\mathbf{n+1}} = \boldsymbol{T}^{\mathbf{n}} + \boldsymbol{b}. \tag{7}$$

$\bar{\bar{\boldsymbol{M}}}$ is a sparse band matrix, $\boldsymbol{T}^{\mathbf{n+1}}$ and $\boldsymbol{T}^{\mathbf{n}}$ the vectors of the temperature field for the next and current time step, respectively, and vector $\boldsymbol{b}$ contains the boundary conditions. The linear system is solved by the Matlab® routine mldivide which is part of a DLR in-house tool for sizing regenerator type thermal energy storages.

Model Validation

The model is validated with experimental data provided by Hoffmann et al. (*17*). Figure 2 gives an example with experimental data of the SolarOne project in comparison with the simulated temperature profiles at 4 and 8 hours from the beginning of the simulation. The simulated storage had 170 MWth power with 18.2 m in diameter and 12 m in height. As heat transferring fluid (HTF) a thermal oil, Caloria® HT 43, was used. The storage was filled with granite and sand, having a porosity of 22 % and 4.6 mm average particle diameter. The mass flow was set to 23 kg/s with 179.2 °C discharging temperature. In the given example, the storage volume is discretized with 400 nodes and 60 s time step length. It can be seen, that the data from SolarOne project largely agrees with modelling data of this work. In addition, other experimental data given by Hoffman et al. has been used to validate our model as well.

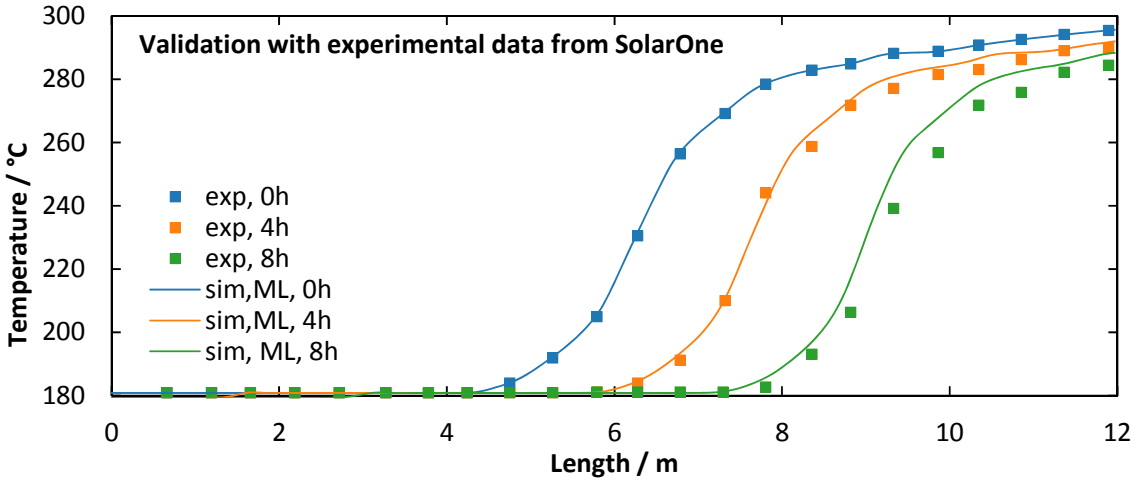

FIGURE 2. Comparison of simulated spatial temperature profile with experimental data of the SolarOne project

Measures for the Rating of the TESIS Test Facility

The model is used to simulate the thermal behavior of the TESIS test facility with different geometry of the packing material and permitted change of the exit temperature during charging and discharging process. As already described in the introduction, the latter effect has particular importance and therefore will be given special attention.

To compare different storage configurations and operation strategies, an exergetic efficiency Ξ is used. That is the actual exergy extracted from the storage volume during discharge $\Delta E''_{\mathrm{stor}}$, divided by the maximum available exergy during the charging process under nominal conditions $\Delta E'_{\mathrm{stor,nom}}$.

$$\Xi = \frac{\Delta E''_{\mathrm{stor}}}{\Delta E'_{\mathrm{stor,nom}}} = \frac{\int_0^{t''_{\mathrm{e}}} \dot{m}'' \cdot \left[h\left(T''_{\mathrm{in,nom}}\right) - h\left(T''_{\mathrm{out}}(t)\right) - T_{\mathrm{u}} \cdot \left(s\left(T''_{\mathrm{in,nom}}\right) - s\left(T''_{\mathrm{out}}(t)\right)\right)\right] dt}{\int_0^{t'_{\mathrm{e}}} \dot{m}' \cdot \left[h\left(T'_{\mathrm{in,nom}}\right) - h\left(T'_{\mathrm{out,nom}}\right) - T_{\mathrm{u}} \cdot \left(s\left(T'_{\mathrm{in,nom}}\right) - s\left(T'_{\mathrm{out,nom}}\right)\right)\right] dt}. \tag{8}$$

The superscript $'$ generally indicates the charging cycle whereas $''$ the discharging cycle. The time of reaching the end of a cycle is denoted by t_{e}. By using the nominal conditions during charging instead of the actual stored exergy, higher emphasis is laid into the storing capabilities. If the efficiency was based on the actually stored exergy, a storage volume with poor storing efficiency could still have a good overall efficiency. The thermal utilization η is calculated from difference of the mean inner energy $\bar{u}_{\mathrm{sf}}$ of the storage volume (i.e. mean of the solid and fluid) at the beginning and the end of the discharging process, which is then based on the maximum storable energy.

$$\eta = \frac{Q''(t''_{\mathrm{e}})}{Q''(t''_0)} = \frac{m \cdot \frac{1}{L} \int_0^L \left[\bar{u}_{\mathrm{sf}}\left(T(x, t''_{\mathrm{e}})\right) - \bar{u}_{\mathrm{sf}}\left(T(x, t''_0)\right)\right] dx}{m \cdot \left[\bar{u}_{\mathrm{sf}}\left(T''_{\mathrm{in,nom}}\right) - \bar{u}_{\mathrm{sf}}\left(T''_{\mathrm{out,nom}}\right)\right]}. \tag{9}$$

SIMULATION AND RATING OF THE TESIS TEST FACILITY

The results described in the following chapters are calculated with the Matlab-model. The results presented here are all for the cyclic steady state. This means, that the storage volume has run through multiple charging and discharging cycles until the duration of two consecutive charging or discharging cycles has not been changed for at least 20 cycles.

Influence of Various Parameters

In the following investigations, the parameters given by Tab. 1 are considered. The measures of the tank are fixed to 5.76 meters of the effective bed length and 2.20 m diameter, resulting in 3.82 m^2 free flow area. Mass flow rate is fixed to 4 kg/s and the nominal inlet temperatures are fixed to 560 °C during charging and 290 °C during discharging, respectively. For the packing material thermophysical properties of basalt are assumed (*18*). The geometry of the packing material, however is subject to investigations, hence the average particle diameter is varied from 3 mm to 50 mm in 3 mm steps and the porosity from 24 % to 40 % in 4 % steps. Also, the maximum permitted change in exit temperature ΔT_e is subject to variations. In a first study, ΔT_e is varied from 10 to 100 Kelvin with 30 K steps for both the charging and discharging cycle. In a second study ΔT_e for the charging process is fixed to 10 K but varied for the discharging process.

TABLE 1. Parameters for the current study

Description	**Value**	**Unit**
Length of the storage tank (L)	5.76	m
Free flow area of the storage tank (A_0)	3.82	m^2
Particle diameter (d_{part})	3 – 50	mm
Porosity (ε)	24 – 40	%
Nominal charging temperature ($T'_{in,nom}$)	560	°C
Nominal discharging temperature ($T''_{in,nom}$)	290	°C
Mass flow rate ($\dot{m}$)	4.0	kg/s
Packing Material	basalt	-
Heat Transfer Fluid (HTF)	solar salt	-
Study 1		
Maximum permitted exit temperature drop (ΔT_e)	10 – 100	K
Study 2		
Maximum permitted exit temperature drop during charging ($\Delta T'_e$)	10	K
Maximum permitted exit temperature drop during discharging ($\Delta T''_e$)	10 – 100	K

The results of the variation of the porosity and maximum permitted temperature drop are shown in Fig. 3, where the following conclusions can be drawn:

- In all cases it is beneficial having the smallest possible packing material. Hence, only 3 mm particles are considered in the following discussion.
- The highest pressure loss would be induced by the smallest particles of 3 mm. Lower porosities than 40 % can only be achieved by a mixture of larger and smaller particles. Therefore, it is assumed that in the 24 % porosity case the bed is filled with larger particles having 40 % porosity and the 3 mm particles fill the gaps in between. As proven by Bruch et al. (*5*), only the smallest (3 mm) particles contribute to the pressure loss. Hence, the pressure loss in our case is independent of the porosity. With this assumption, the maximum pressure loss is 516 Pa. That means, in terms of pumping power, all configurations are uncritical. However, higher pressure losses contribute to an improved flow distribution.

- Except for the pressure losses, there is virtually no impact of the porosity on the results. Therefore, it is favorable having the lowest possible porosity, which causes a low holdup of the more expensive molten salt.
- If the permitted change in exit temperature is low,
    - the constantly high level of the exit temperature causes a high exergetic efficiency, but
    - the thermocline region expands during operation of charging and discharging until a quasi-steady operation is reached. Due to its larger width, the thermocline region can move only smaller distances until it reaches the exit and the maximum permitted change in exit temperature is reached.

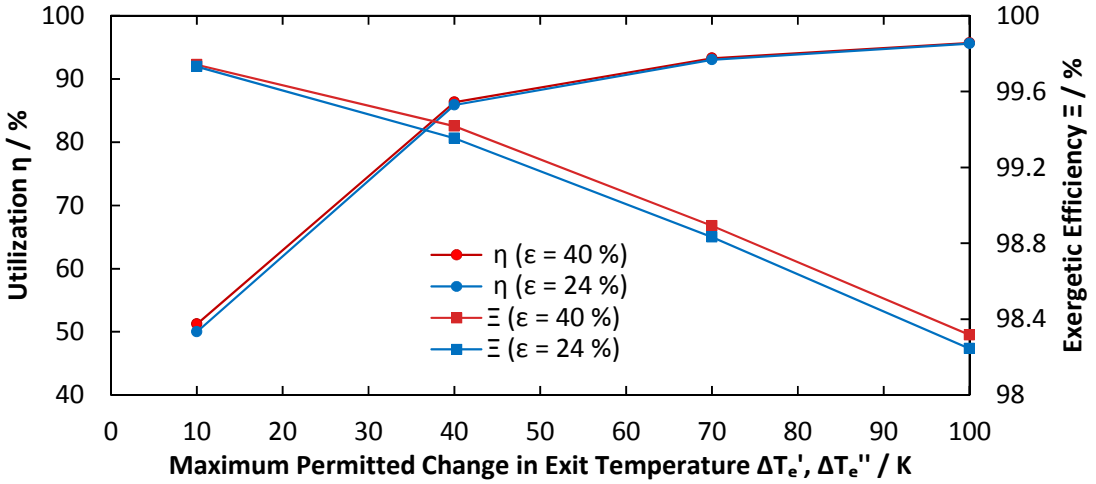

FIGURE 3. Study 1: Effect of porosity and maximum permitted change in exit temperature on the utilization and exergetic efficiency of the storage volume

For the above simulations in study 1, a symmetric operation strategy, i.e. the maximum permitted change in exit temperature is the same for both charging and discharging has been considered. Higher permitted change in exit temperature increases utilization but causes also lower exergetic efficiencies.

The reason for the better utilization when allowing higher permitted change in exit temperature lies in the moment of switching between the periods. In that moment, the temperature difference between filler and inflowing molten salt is high, which narrows the thermocline region.

Optimized Operation Strategy

In study 2, the permitted change in exit temperature is held constant at 10 Kelvin for the charging cycle and varied for the discharge cycle. The results are shown in figure 4. For a better comparison, the results from study 1 are shown as well.

When comparing the results of both studies, it can be seen that if the permitted change in exit temperature increases,

- the exergetic efficiency remains nearly constant this time. First, during charging, the exit temperature remains almost constant, since it drops only by 10 Kelvin. Hence, when compared to the cases with higher permitted change in exit temperature from study 1, the storage can store more exergy and energy. During discharge, the exit temperature can drop further down which causes a slightly longer discharge period than the charging period. This, in turn, increases the exergetic efficiency at the same permitted change in exit temperature in study 2 when compared to study 1.
- The low permitted change in exit temperature during charging prevents the thermocline from being shortened during the switching from charging to discharging. Therefore, the utilization decreases.

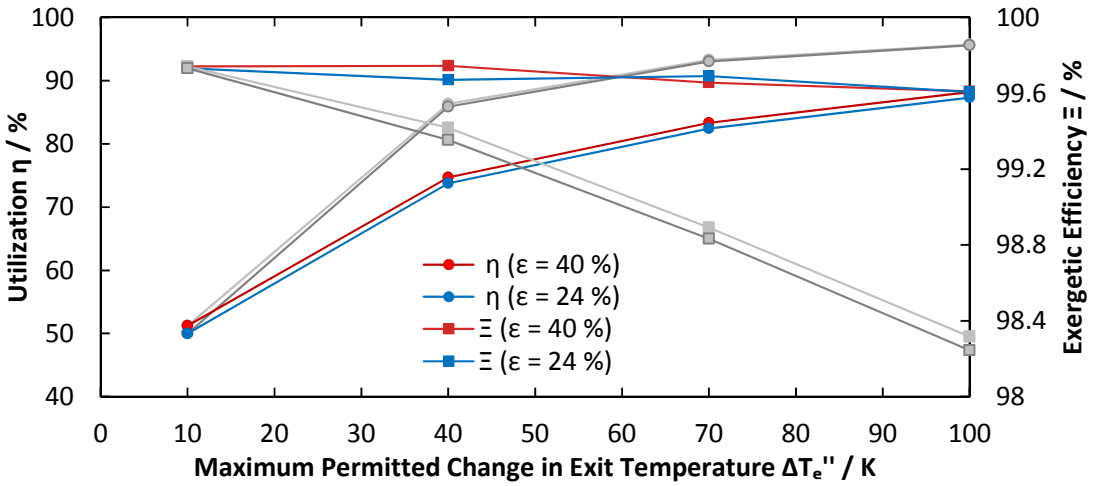

FIGURE 4. Study 2: Effect of maximum permitted change in exit temperature during discharging on the utilization and exergetic efficiency of the storage volume in comparison to study 1 in grey color

As can be seen from study 2, an asymmetric operation strategy can further increase the exergetic efficiency at the cost of the storage utilization.

Summary

From the simulations it becomes evident, that significant temperature differences in the inlet region of the storage volume at the beginning of a new thermal cycle are beneficial for a short thermocline zone. This is achieved by high permitted changes in exit temperature, which strongly depends on the later attached process to the storage volume. On the one hand, such a short thermocline both increases the utilization of the storage volume and keeps the exit temperature at maximum for a longer period. On the other hand, higher changes of the exit temperature cause increased exergy destruction as well.

Based on the findings, a possible improved operation strategy for the TESIS:store thermocline test facility could be an asymmetric operation with small change in permitted exit temperature during charging and larger change in exit temperature during charging. This can improve the exergetic efficiency. The approach of asymmetric operation presented in this paper bears further potential for optimization of effective thermocline operation by varying both charging and discharging permitted exit temperature levels.

In terms of the possible filler material, the lowest possible porosity and particle diameter should be used. There might be further limitations due to flow distribution, dust contamination or other effects such as ratcheting which are subject to further investigations.

ACKNOWLEDGMENTS

The authors thank the German Federal Ministry for Economic Affairs and Energy for the financial support given for this work in the MS-STORE project (Contract No. 0325497 A).

REFERENCES

1. C. Libby, “Solar Thermocline Storage Systems: Preliminary Design Study” (2010), , doi:Report no. 1019581, EPRI, California.
2. S. E. Faas, L. R. Thorne, N. D. Fuchs, E.A. ; Gilbertsen, “10 MWe Solar Thermal Central Receiver Pilot Plant: Thermal Storage Subsystem Evaluation Final report” (1986).
3. J. E. Pacheco, S. K. Showalter, W. J. Kolb, Development of a Molten-Salt Thermocline Thermal Storage System for Parabolic Trough Plants. *J. Sol. Energy Eng.* **124**, 153 (2002).
4. A. Mawire, M. McPherson, Experimental and simulated temperature distribution of an oil-pebble bed

thermal energy storage system with a variable heat source. *Appl. Therm. Eng.* **29**, 1086–1095 (2009).
5. A. Bruch, J. F. Fourmigué, R. Couturier, Experimental and numerical investigation of a pilot-scale thermal oil packed bed thermal storage system for CSP power plant. *Sol. Energy*. **105**, 116–125 (2014).
6. R. Bayón, E. Rojas, Analytical function describing the behaviour of a thermocline storage tank: A requirement for annual simulations of solar thermal power plants. *Int. J. Heat Mass Transf.* **68**, 641–648 (2014).
7. M. Biencinto, R. Bayón, E. Rojas, L. González, Simulation and assessment of operation strategies for solar thermal power plants with a thermocline storage tank. *Sol. Energy*. **103**, 456–472 (2014).
8. W. Gaggioli, F. Fabrizi, P. Tarquini, L. Rinaldi, Experimental Validation of the Innovative Thermal Energy Storage Based on an Integrated System "storage Tank/Steam Generator." *Energy Procedia*. **69**, 822–831 (2015).
9. E. Rivas *et al.*, CFD model of a molten salt tank with integrated steam generator. *Energy Procedia*. **49**, 956–964 (2013).
10. J. Lata, J. Blanco, Single tank thermal storage design for solar thermal power plants. *SolarPaces Conf.*, 1–9 (2010).
11. S. Rodat, A. Bruch, N. Dupassieux, N. El Mourchid, Unique Fresnel Demonstrator Including ORC and Thermocline Direct Thermal Storage: Operating Experience. *Energy Procedia*. **69**, 1667–1675 (2015).
12. N. Breidenbach, C. Martin, H. Jockenhoefer, T. Bauer, in *IRES 2016* (2016).
13. R. Bayón, E. Rojas, Simulation of thermocline storage for solar thermal power plants: From dimensionless results to prototypes and real-size tanks. *Int. J. Heat Mass Transf.* **60**, 713–721 (2013).
14. F. W. Schmidt, A. J. Willmott, *Thermal energy storage and regeneration* (Hemisphere Publishing Corporation, Washington, D.C., USA, ed. 1, 1981; http://www.dl.begellhouse.com/pt/download/article/541fea952db5c823/HE (571-597).pdf).
15. N. Wakao, S. Kagei, *Heat and mass transfer in packed beds* (Gordon and Breach Science Publishers Inc., New York, 1982).
16. S. Ergun, a. a. Orning, Fluid Flow through Randomly Packed Columns and Fluidized Beds. *Ind. Eng. Chem.* **41**, 1179–1184 (1949).
17. J.-F. Hoffmann, T. Fasquelle, V. Goetz, X. Py, A thermocline thermal energy storage system with filler materials for concentrated solar power plants: Experimental data and numerical model sensitivity to different experimental tank scales. *Appl. Therm. Eng.* **100**, 753–761 (2016).
18. H. Vosteen, R. Schellschmidt, Influence of temperature on thermal conductivity, thermal capacity and thermal diffusivity for different types of rock. *Phys. Chem. Earth*. **28**, 499–509 (2003).